Matrix augmentation as an efficient method for resolving interaction of bromocriptine with human serum albumin: trouble shooting and simultaneous resolution

Ali R. Jalalvand [a,*], Sirous Ghobadi [b], Hector C. Goicoechea [c], Elahe Faramarzi [a], Majid Mahmoudi [a]

[a] Research Center of Oils and Fats, Kermanshah University of Medical Sciences, Kermanshah, Iran
[b] Department of Biology, Faculty of Science, Razi University, Kermanshah, Iran
[c] Laboratorio de Desarrollo Analítico y Quimiometría (LADAQ), Catedra de Química Analítica I, Universidad Nacional del Litoral, Ciudad Universitaria, CC242, S3000ZAA, Santa Fe, Argentina

ABSTRACT

This work reports the results of an interesting study related to the investigation of interactions of bromocriptine (BCP) with human serum albumin (HSA) by mathematicall modelling of voltammetric and spectroscopic data into an augmented data matrix and its resolution by multivariate curve resolution-alternating least squares (MCR-ALS). The quality of the results obtained by MCR-ALS was examined by MCR-BANDS and its outputs confirmed the absence of rotational ambiguities in the MCR-ALS results. BCP-HSA interactions were also modeled by molecular docking methods to verify the results obtained from experimental sections and fortunately, they were compatible. Hard modeling of the experimental data by EQUISPEC helped us to calculate the binding constant of the complex formed from BCP-HSA interactions which was in a good agreement with that of calculated from direct analysis of the experimental data. Finally, with the help of two different amperometric measurements based on BCP-HSA interactions a novel electroanalytical method was developed for biosensing of HSA in serum samples.

1. Introduction

Bromocriptine (BCP, Fig. 1A) as an oral dopamine receptor agonist is used for the therapy of Parkinson disease [1]. The BCP is a strong inhibitor against prolactin formation with therapeutic potency in the treatment of hyperprolactinemia which is also used in the treatment of migraine [2, 3, 4, 5, 6]. The effects mentioned above are observed for BCP because of the ability of BCP to block dopamine receptors and its interaction with calmodulin-induced activation of phosphodiesterases in human brain [7, 8].

Human serum albumin (HSA, Fig. 1B) as the most abundant protein in human blood plasma acts as a carrier for drugs [9, 10, 11, 12, 13, 14, 15]. Free concentration, distribution and metabolism of drugs are highly depended on their interactions with HSA. On the other side, determination of the concentration of HSA is important from clinical point of view, because unusual concentrations of HSA unravel the existence of some diseases such as diabetes and cardiovascular disease, etc. Common methods for determination of HSA include LC-MS/MS, capillary

electrophoresis and immunoassays which suffer from time and cost therefore, developing novel analytical methods for determination of HSA which are fast and low-cost is important from clinical point of view.

Generally, interactions of drugs with HSA are investigated by UV-Vis spectrophotometry [16], FT-IR [17], electrochemistry [18], capillary electrophoresis [19], HPLC [20] and NMR [21]. Sometimes, instrumental techniques are assisted by chemometric methods for investigation of interactions of drugs with HSA [22, 23]. HSA-drug interactions produce a complicated system which its monitoring needs simultaneous monitoring of HSA, drug and their complex product. Simultaneous resolution of such a complex system is quiet challenging therefore, multivariate analysis of the data is demanded. Multivariate curve resolution-alternating least squares (MCR-ALS) is a famous chemometric tool which can help us in resolving HSA-drug interactions to obtain new information about the studied system.

The steps of this work are including: 1) direct analysis of voltammetric and spectroscopic data to obtain some information about BCP-HSA interactions, 2) mathematical modeling of voltammetric and
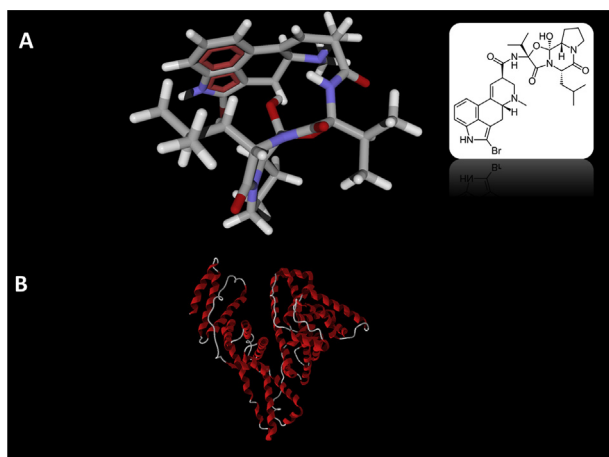

Fig. 1. (A) Molecular structure of BCP and (B) secondary structure of HSA.

spectroscopic data to construct an augmented data matrix and its simultaneous resolution by MCR-ALS for obtaining new information about BCP-HSA interactions, 3) modeling of BCP-HSA interactions by molecular docking methods and 5) developing a novel electroanalytical methodology for electrochemical biosensing of electro-inactive HSA.

2. Experimental

2.1. Experimental details

2.1.1. Chemicals and solutions

HSA, BCP, warfarin (Wr), ibuprofen (Ip), acetic acid, ethanol, dimethylformamide (DMF), sodium phosphate monobasic (NaH_2PO_4), sodium phosphate dibasic (Na_2HPO_4), 1-ethyl-3-methylimidazolium bis(trifluoromethylsulfonyl)Imide (IL), dimethyl sulfoxide (DMSO), sodium hydroxide, phosphoric acid (H_3PO_4), sodium chloride and hydrochloric acid were purchased from Sigma. Ionic Liquid Technologies was chosen as a well-known brand to purchase multiwalled carbon nanotubes (MWCNTs). Other chemicals were prepared from legal sources. A 0.05 M phosphate buffer solution (PBS) was prepared from NaH_2PO_4 and Na_2HPO_4 and its pH was adjusted at 7.4 by H_3PO_4 and NaOH. Stock solutions of BCP and HSA with a were prepared in the PBS (0.05 M, pH 7.4) and stock solutions of Wr and Ip were prepared in DMSO. To prepare MWCNTs-IL, 30 mg MWCNTs was added to 1 mL DMF+50 μL IL and ultrasonicated for 45 min. All the solutions were prepared by doubly distilled water (DDW).

A medical diagnostic laboratory provided us three human serum samples which were centrifuged at 4500 rpm for 20 min and the supernatants were discarded. To 5 mL of each sample was 45 mL PBS (0.05 M, pH 7.4) was added and then, each sample was analyzed towards determination of HSA.

2.1.2. Instruments and softwares

All the electrochemical data were collected by an Autolab PGSTAT302N-high performance controlled by the NOVA 2.1.2 software. Electrochemical experiments were performed in an electrochemical cell containing a bare or modified glassy carbon electrode (GCE), a Pt wire and an Ag/AgCl electrode acted as working, counter and reference electrode, respectively. A KYKY-EM 3200 scanning electron microscope was used to take the SEM images. A Cary Eclipse fluorescence spectrophotometer equipped with a water bath and a 1.0 cm quartz cell was used to record the spectrofluorimetric data. A Shimadzu spectrophotometer equipped with a 1.0 cm quartz cell was used to collect the spectrophotometric data. pH adjustments were performed by an ELMEIRON pH-

meter (CP-411). Molecular structure of the BCP was depicted and optimized by Hyperchem. The PDB file of HSA (PDB Id: 1AO6) was downloaded from Brookhaven Protein Data Bank (PDB). For docking of BCP to HSA, Arguslab software was used. LIGPLOT an automatically program for plotting protein-ligand interactions [24], was used to plot BCP-HSA interactions. The routines of MCR-ALS and MCR-BANDS were available in internet [25].

2.1.3. Fabrication of the modified electrodes

A bare GCE was well polished by a silky polishing pad and then, rinsed with DDW and dried at room temperature. By drop-casting of 10 μL HSA 10^{-4} M to the surface of the cleaned bare GCE, the HSA/GCE was fabricated. To fabricate MWCNTs-IL/GCE, 10 μL MWCNTs-IL was drop-casted onto the surface of the cleaned GCE. The SEM images of HSA/GCE and MWCNTs-IL/GCE are shown in Fig. 2.

2.1.4. Procedures

For performing each spectroscopic experiment, different volumes of HSA or BCP were added to a quartz cell containing 2 mL of HSA or BCP with a known concentration. Each solution was shaken for 15 s and then, its spectrum was recorded.

In each voltammetric experiment, 4 mL of HSA or BCP with a known concentration was added to the electrochemical cell and different volumes of HSA or BCP was added to the cell. Each solution was genteely stirred for 1 min and then, its voltammogram was recorded.

2.1.5. Experiments required to build an augmented data matrix

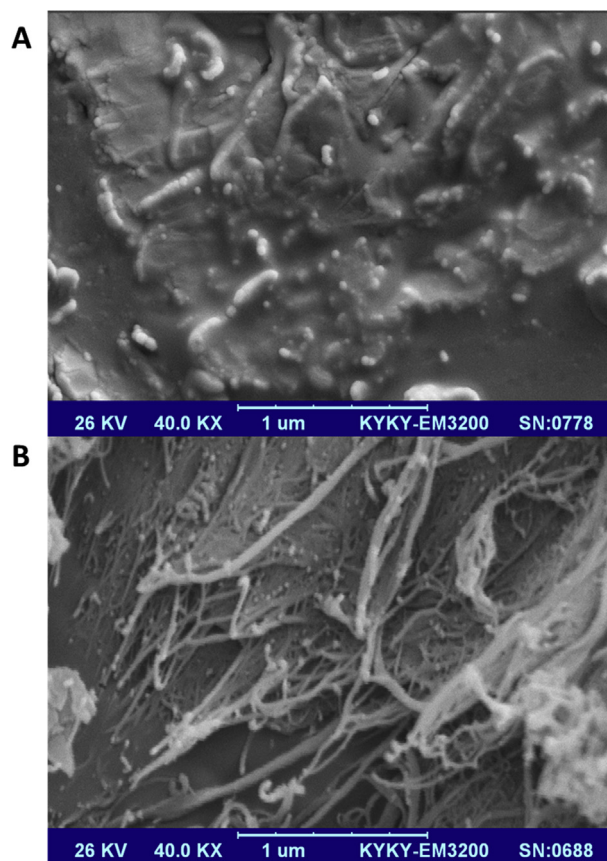All the experiments used to build an augmented matrix have been codded in Table 1.

Fig. 2. The SEM images captured from the surface of (A) HSA/GCE and (B) MWCNTs-IL/GCE.

Table 1
Experimental coding used in this study.

Data Matrix	Species with constant concentration	Species with varying concentration	Instrumental technique
D_F^{HSA}	HSA, 2.0×10^{-7} M	BCP, 0–1.0×10^{-6} M	Fluorescence
D_{UVVis}^{HSA}	HSA, 1.0×10^{-5} M	BCP, 0–5.0×10^{-5} M	UVVis
D_{DPV}^{HSA}	HSA, 1.0×10^{-5} M	BCP, 0–5.0×10^{-5} M	Differential pulse voltammetry
D_{LSV}^{HSA}	HSA, 1.0×10^{-4} M	BCP, 0–5.0×10^{-4} M	Linear sweep voltammetry
D_{CV}^{HSA}	HSA, 1.0×10^{-4} M	BCP, 0–5.0×10^{-4} M	Cyclic voltammetry
D_F^{BCP}	BCP, 1.0×10^{-7} M	HSA, 0–1.0×10^{-7} M	Fluorescence
D_{UVVis}^{BCP}	BCP, 1.0×10^{-4} M	HSA, 0–1.0×10^{-4} M	UVVis
D_{DPV}^{BCP}	BCP, 1.0×10^{-5} M	HSA, 0–1.0×10^{-5} M	Differential pulse voltammetry
D_{LSV}^{BCP}	BCP, 1.0×10^{-4} M	HSA, 0–1.0×10^{-4} M	Linear sweep voltammetry
D_{CV}^{BCP}	BCP, 1.0×10^{-4} M	HSA, 0–1.0×10^{-4} M	Cyclic voltammetry

3. Theory

3.1. Required information about application of MCR-ALS to the augmented data matrix

There are some works published on application of MCR-ALS in the analysis of electroanalytical data [26, 27, 28, 29] and in this section, a summarized description is dedicated. A voltammetric or spectroscopic data matrix (D (M×N), M objects and N variables e.g. wavelength or potential) can be decomposed by MCR to obtain spectra or voltammograms and concentration profiles according to the following equation:

$$D = CS^T + E \tag{1}$$

where C is a (M×P) matrix which contains concentration profiles of the P species, S^T is a (P×N) matrix containing pure signals and E is a (M×N) matrix which contains residuals. After decomposition of D, ALS as one of the most important iterative approaches is used to optimize the results of MCR. Resolution of a chemical system monitored by more than one instrumental technique by MCR-ALS needs a column- and row-wise augmented data matrix. In this work, BCP-HSA interactions have been investigated by differential pulse voltammetry (DPV), linear sweep voltammetry (LSV), cyclic voltammetry (CV), UVVis spectrophotometry and fluorescence spectroscopy (F). The individual data matrices related to the instrumental techniques were augmented into a matrix according to the following equation:

where D_{DPV}, D_{LSV}, D_{CV}, D_{UVVis} and D_F refer to the data recorded by DPV, LSV, CV, UVVis and F. C, S and E are concentration, pure signals and residuals, respectively.

Evolving Factor Analysis (EFA) can be used to determine the number of species (P) of the augmented data matrix [30, 31, 32], and to obtain an initial estimation of the concentration profiles. Some constraints are used during ALS optimization which help to obtain chemically meaningful results [33]. The lack of fit (*lof*) is a criterion to evaluate the quality of the final results. The *lof* is the difference between the input data (D) and the data reproduced by MCR-ALS which can be calculated according to the following equation [34]:

$$lof\ (\%) = 100\sqrt{\frac{\sum_{i,j} e_{i,j}^2}{\sum_{i,j} d_{i,j}^2}} \tag{3}$$

where d_{ij} is an element of D and e_{ij} is its corresponding residual.

The solutions which are applied to solve Eq. (1) by MCR-ALS are not unique and may have some rotational and intensity ambiguities. Column- and row-wise augmentation can be used to shooting this trouble. Matrix augmentation which help us to simultaneous resolution of different types of instrumental data is more powerful than that described by Eq. (1) and can be used as an efficient strategy for simultaneous resolution of complex data and to cope with the challenge arising from the small signal shifts observed in the data. However, because of combination of different types of instrumental data, some considerations as follows must not be neglected:

1. Voltammetric and spectroscopic data have different intensities therefore, normalization of them is required for having similar weight on the iterative ALS optimization. This goal can be achieved by dividing each matrix to its maximum value.
2. The augmented matrix which is used as the input of MCR-ALS contains different types of instrumental data therefore, in this case, the concept of component is complicated. From spectroscopic and voltammetric point of view a component has different meanings. From spectroscopic point of view, a component is a pure chemical species in solution [35, 36], but from electrochemical point of view a component which is associated to a single electrochemical process can also be associated adsorption at the electrode surface or capacitive currents [37, 38].
3. For building an augmented data matrix by the association of individual voltammetric and spectroscopic matrices, size of all the matrices must be equal and a same distribution of the species during all the experiments is needed. To achieve this goal, a same total concentration is needed for BCP and HSA in all titrations, but achieving to this goal is impossible because higher concentrations are needed for voltammetric experiments than spectroscopic experiments. Therefore, to achieve the goal mentioned above, all the voltammetric and spectroscopic experiments have been performed at different total concentrations but with the same values of ratio.

4. Results and discussion

4.1. Voltammetric studies of BCP-HSA interactions

4.1.1. Cyclic voltammetry

CV as a powerful electrochemical has been frequently used to investigate interactions of small molecules with serum albumin [39], therefore, we used it to investigate BCP-HSA interactions. To achieve this goal,

$$\begin{bmatrix} D_{DPV}^{BCP} D_{LSV}^{BCP} D_{CV}^{BCP} D_F^{BCP} D_{UVVis}^{BCP} \\ D_{DPV}^{HSA} D_{LSV}^{HSA} D_{CV}^{HSA} D_F^{HSA} D_{UVVis}^{HSA} \end{bmatrix} = \begin{bmatrix} C^{BCP} \\ C^{HSA} \end{bmatrix} \begin{bmatrix} S_{DPV}^T S_{LSV}^T S_{CV}^T S_F^T S_{UVVis}^T \end{bmatrix} + \begin{bmatrix} E_{DPV} E_{LSV} E_{CV} E_F E_{UVVis} \end{bmatrix} \tag{2}$$

HSA in the range of 0–1.0×10^{-4} M was added to a constant concentration of BCP (1.0×10^{-4} M) and the results are shown in Fig. 3A. As can be seen, the CV response of the BCP is affected by the addition of HSA which its peak current and peak potential were decreased and increased, respectively. These phenomena are related to the interactions of BCP with HSA and change in the molecular environment around the BCP molecule [40]. E_p and $E_{p/2}$ values of the CV response of the BCP at the GCE surface are 270 and 170 mV, respectively. For an irreversible oxidation $|E_p - E_{p/2}| = 47.7/\alpha n$ [41], and $\alpha = 0.5$ [42], n was calculated to be 2.07 i.e. ~ 1.

Some information about the type of interactions of a small molecule with a biological macromolecule could be obtained by immobilizing the biomacromolecule onto the electrode surface [43, 44]. To achieve this goal, the response of GCE to BCP (curve *a*) was compared with that of
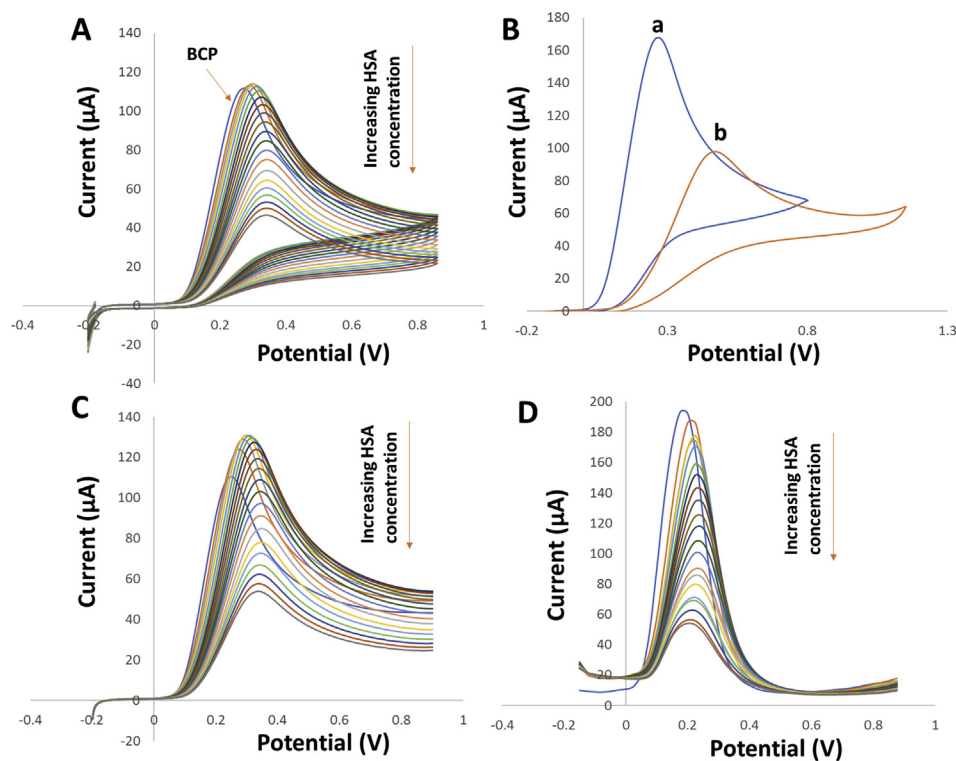
Fig. 3. (A) CVs of 1.0×10^{-4} M BCP in the presence of increasing concentration of HSA in the range of 0–1.0×10^{-4} M, (B) CVs of 2.0×10^{-4} M BCP recorded at the surface of bare GCE (curve a) and HSA/GCE (curve b), (C) LSVs of 1.0×10^{-4} M BCP in the presence of increasing concentration of HSA in the range of 0–1.0×10^{-4} M and (D) DPVs of 1.0×10^{-5} M BCP in the presence of increasing concentration of HSA in the range of 0–1.0×10^{-5} M.
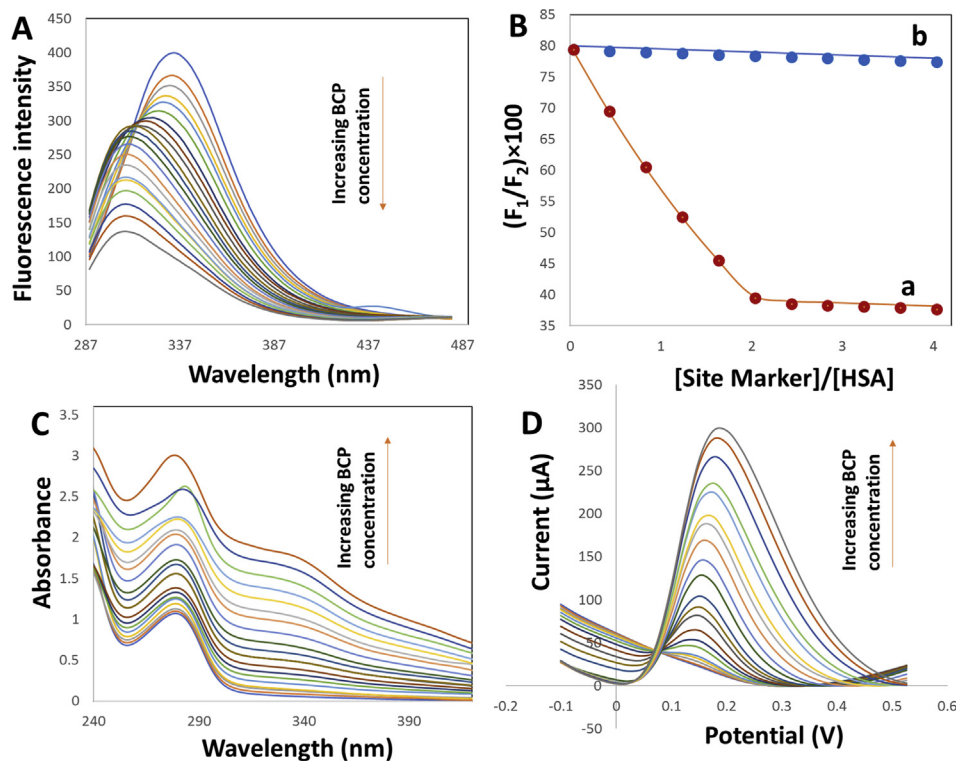

Fig. 4. (A) Fluorescence emission spectra of 2.0×10^{-7} M HSA ($\lambda_{ex} = 280$ nm) in the presence of increasing concentration of BCP ranging in 0–1.0×10^{-6} M, (B) effects of Wr (curve a) and Ip (curve b) as site markers on the fluorescence of HSA-BCP, (C) UVVis absorption spectra of 1.0×10^{-5} M HSA in the presence of increasing concentration of BCP ranging in 0–5.0×10^{-5} M and (D) DPVs of 1.0×10^{-5} M HSA in the presence of increasing concentration of BCP ranging in 0–5.0×10^{-5} M.

HSA/GCE (curve *b*), and the results are shown in Fig. 3B. As can be seen, the CV response of BCP at the surface of HSA/GCE was observed at more positive potentials than its response at bare GCE. The positive shifts observed in the CV response of BCP at the surface of HSA/GCE confirmed that the main interactions of BCP with HSA were hydrophobic interactions [43].

The binding of BCP to HSA/GCE was also investigated by recording the CV responses of HSA/GCE to different concentrations of BCP (not shown). The CVs' intensities were increased with increasing BCP concentration (C_{BCP}) and subsequently were reached to saturation values. According to Eq. (4) [45], in which *I*, I_{max}, and K_b are referred to peak current, maximum peak current and binding constant of BCP to HSA/GCE surface, respectively, C_{BCP}/I on were regressed on C_{BCP} (not shown) to obtain the K_b value which was calculated to be 5.08×10^5 mol^{-1} L.

$$C_{BCP}/I = (1/K_b I_{max}) + (C_{BCP}/I_{max}) \qquad (4)$$

4.1.2. LSV and DPV studies

The LSV and DPV studies of of BCP-HSA interactions were performed by recording the instrumental signals at GCE obtained by adding HSA to BCP and the results are shown in Fig. 3C and D, respectively. As can be seen, the intensity of the CV response of the BCP was decreased and shifted to more positive potentials by the addition of HSA which may be related to the embedding of BCP within the HSA structure and its interaction with HSA or a competitive adsorption may be occurred at the GCE surface. As reported by the other researchers [46, 47], a low area from the electrode surface (10%) is covered by the interaction of a low concentration of a biological macromolecule such as HSA with a small molecule therefore, adsorption can be neglected and the mentioned phenomena are related to the interaction of BCP with HSA, but in next section our studies will ne assisted by chemometric methods to obtain more information about BCP-HSA interactions.

4.2. Spectroscopic studies

4.2.1. Spectrofluorimetric studies

The spectrofluorimetric data obtained by the titration of 2.0×10^{-7} M HSA prepared in the PBS (0.05 M, pH 7.4) upon addition of BCP in the range of $0.0-1.0 \times 10^{-6}$ M at three different temperatures (i.e., 298.15, 304.15 and 310.15 K) were recorded and one of them (298.15 K) is shown in Fig. 4A. The results showed that the fluorescence intensity of HSA was decreased versus increasing concentration of BCP. The intrinsic fluorescence of HSA is related to its single tryptophan residue (Trp-214) whose intensity is decreased by the interaction of a small molecule with HSA [48, 49, 50]. Fluorescence quenching can be caused by different molecular interactions such as energy transfer, molecular rearrangements, excited state reactions, complex formation and collisional quenching, but fluorescence quenching is usually occurred by dynamic collision and static quenching (complex formation). Usually, Stern-Volmer equation is used to clarify the mechanism of fluorescence quenching [51]:

$$F_0/F = 1 + K_{SV}[Q] \qquad (5)$$

where F_0 and *F* are steady-state fluorescence intensities in the absence and presence of the BCP as quencher (*Q*), respectively. K_{SV} and [*Q*] are the Stern-Volmer quenching constant and concentration of the BCP,

Table 2
Stern-Volmer quenching constants at different temperatures related to BCP-HSA interactions.

T (K)	K_{SV} ($\times 10^5$ L mol^{-1})	R^2
298.15	4.96	0.991
304.15	4.31	0.998
310.15	3.94	0.992

respectively. According to Eq. (5), the results of regression of F_0/F values on [*Q*] (not shown), are presented in Table 2. As can be seen, the K_{SV} values are decreased with increasing temperature suggesting a static quenching (complex formation) for BCP-HSA interactions.

4.2.2. Site selectivity of binding of BCP to HSA

There are two sites including site I (hydrophobic sub-domain IIA) [52] and Sudlow's sites II (sub-domain IIIA) [53] in HSA which enable small molecules for binding with HSA. To clarify the location of binding of BCP to HSA, two competitive experiments were designed where two site markers including Wr (marker of site I) and Ip (marker of site II) were used to compete with BCP for binding with HSA. To perform these experiments, Wr or Ip in the range of $0.0-2.0 \times 10^{-7}$ M was added to a mixture containing both of BCP and HSA in which BCP concentration (2.0×10^{-7} M) was four times higher than HSA (5.0×10^{-8} M). Then, (F_1/F_2) × 100 values (F_1 and F_2 are the fluorescence intensity in the absence and presence of site marker, respectively) were plotted versus [Site Marker]/[HSA] as shown in Fig. 4B. As can be seen, the (F_1/F_2) × 100 was decreased by the addition of Wr to the HSA-BCP solution (Fig. 4B, curve *a*) which showed BCP-HSA interactions were affected by the addition of Wr. While, the mentioned system was not affected by the addition of Ip (Fig. 4B, curve *b*) which indicated that the Ip did not compete with BCP for binding with HSA. According to the results mentioned above, we can conclude that the hydrophobic pocket in sub-domain IIA of HSA is the main location for binding of BCP with HSA.

4.2.3. Spectrophotometric studies

UVVis spectrophotometric experiments were also used to investigate of BCP-HSA interactions. Spectrophotometric spectra were recorded by the addition of BCP in the range of $0.0-5.0 \times 10^{-5}$ M to a constant concentration of HSA (1.0×10^{-5} M) and the results are shown in Fig. 4C. An absorption peak observed at 280 nm is related to HSA whose position and intensity were changed in the presence of BCP which were related to interactions of BCP with HSA.

4.2.4. Fluorescence energy transfer from HSA to BCP

Fluorescence energy transfer (FRET) is a global technique for the measurement of molecular distance [54]. Eq. (6) describes efficiency (*E*) of FRET which is depended on inverse sixth power of the distance between donor and acceptor (*r*, Forster distance) [55], Forster radius (R_0, Eq. (7)), overlapping of emission and absorption of donor and acceptor, respectively, and orientation of donor's transition dipole.

$$E = 1 - \frac{F}{F_0} = \frac{R_0^6}{(R_0^6 + r^6)} \qquad (6)$$

$$R_0^6 = 8.8 \times 10^{-25} k^2 n^{-4} J\Phi \qquad (7)$$

k^2, *n*, Φ and *J* have their conventional meaning and *J* can be calculated according to the following equation:

$$J = \frac{\int_0^\infty F(\lambda)\varepsilon(\lambda)\lambda^4 d\lambda}{\int_0^\infty F(\lambda)d\lambda} \qquad (8)$$

where $F(\lambda)$ and ε are the fluorescence intensity of the donor and molar absorption coefficient of the acceptor, respectively. According to the previous work [56] reported in the literature, k^2, *n* and Φ are 2/3, 1.336 and 0.118, respectively, which were used to calculate the values of *J*, R_0, *E* and *r* which were to be 4.36×10^{-14} cm^3M^{-1}, 3.13 nm, 0.08 and 4.7 nm, respectively. According to the values calculated for *r* which is less than 8 nm we can conclude that the energy transfer can be occurred from HSA to BCP [57].

4.3. Building an augmented data matrix

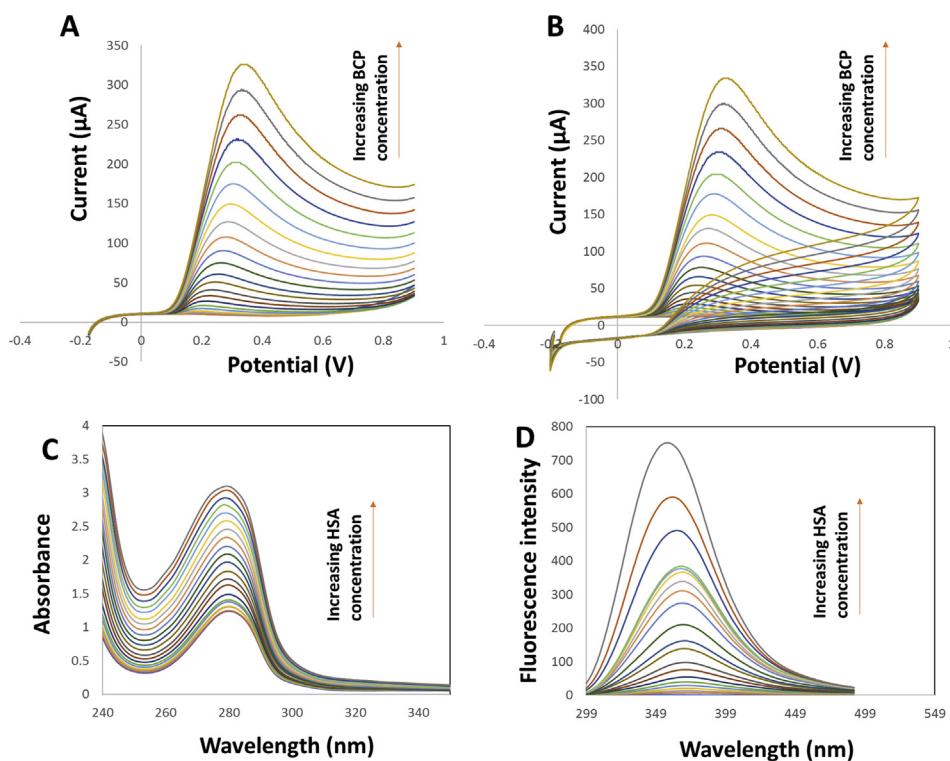In this section, spectroscopic and voltammetric data were collected

Fig. 5. (A) LSVs of 1.0×10^{-4} M HSA in the presence of increasing concentration of BCP ranging in $0-5.0 \times 10^{-4}$ M, (B) CVs of 1.0×10^{-4} M HSA in the presence of increasing concentration of BCP ranging in $0-5.0 \times 10^{-4}$ M, (C) UVVis absorption spectra of 1.0×10^{-4} M BCP in the presence of increasing concentration of BCP ranging in $0-1.0 \times 10^{-4}$ M BCP and (D) fluorescence emission spectra of 1.0×10^{-7} M BCP in the presence of increasing concentration of HSA ranging in $0-1.0 \times 10^{-7}$ M.

into an augmented data matrix described by Eq. (2) and analysed by MCR-ALS which will be more explained in next sections.

4.3.1. MCR-ALS results

Interactions of BCP-HSA were further investigated by MCR-ALS which helped us to obtain more information about stoichiometry of the complex species involved and the relative concentrations of the various species. This goal was achieved by building a column- and row-wise augmented data matrix by collecting data matrices obtained by DPV ($\boldsymbol{D}_{DPV}^{BCP}$, Fig. 3D, $\boldsymbol{D}_{DPV}^{HSA}$, Fig. 4D), LSV ($\boldsymbol{D}_{LSV}^{BCP}$, Fig. 3C, $\boldsymbol{D}_{LSV}^{HSA}$, Fig. 5A), CV ($\boldsymbol{D}_{CV}^{BCP}$, Fig. 3A, $\boldsymbol{D}_{CV}^{HSA}$, Fig. 5B), UVVis ($\boldsymbol{D}_{UVVis}^{BCP}$, Fig. 4C, $\boldsymbol{D}_{UVVis}^{HSA}$, Fig. 5C) and F ($\boldsymbol{D}_{F}^{HSA}$, Fig. 4A, $\boldsymbol{D}_{F}^{BCP}$, Fig. 5D) and then, the augmented data matrix was analysed by MCR-ALS.

The first step was including determination of the number of species by singular value decomposition (SVD) and which detected three main species and we guess that they may be related to BCP, HSA and one HSA-BCP$_m$ complex species. The second step was devoted to find an initial estimation of the concentration profiles with the help of EFA. The EFA is able to work with full rank data sets and is not able to find useful information by the analysis of rank-deficient data and matrix augmentation

can tackle this trouble [58]. In MCR-ALS application of constraints during ALS optimization can help us to obtain reliable results. In this work, due to having CV data which contain negative values, the non-negativity constraint can only apply to the concentration profiles. Because of recording data matrices at different concentration levels, a closure constraint cannot be applied. The ALS was begun for optimizing the MCR results with the help of constraints mentioned above and the *lof* was used as a criterion to evaluate the goodness of the fitting model and here, the *lof* was found to be 3.60% which is an acceptable value for explaining almost all of the variability in the experimental data.

The results of MCR-ALS are shown in Figs. 6 and 7. Fig. 6A and B show the concentration profiles of the species involved and from Fig. 6A it can be concluded that by the addition of HSA to BCP, concentration of BCP is decreased and a complex species is formed whose concentration is increased and reached equilibrium at the ratio of [HSA]/[BCP]~0.5. The maximum concentration of the complex species at [HSA]/[BCP]~0.5 confirms this species is a HSA-BCP$_2$ complex specie. By casting a look at Fig. 6B it can be seen that the ratio of [BCP]/[HSA]~2 is critical in which concentration of the BCP reaches to a minimum while concentrations of HSA and complex species are sharply decreased and increased,
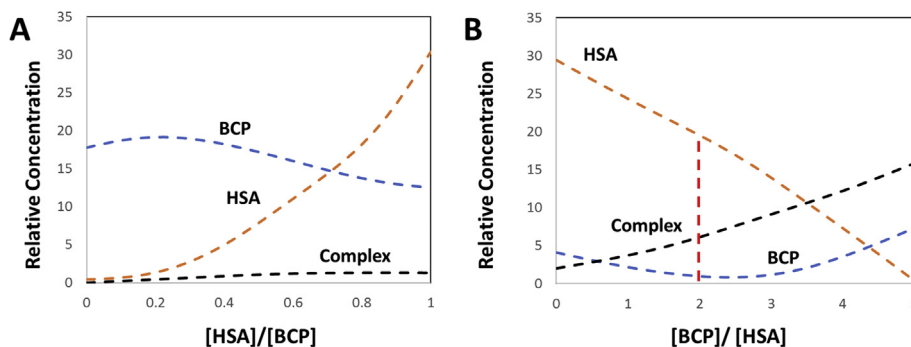

Fig. 6. (A) and (B) concentration profiles of the species involved which were extracted by applying MCR-ALS to the augmented data matrix for simultaneous resolution of voltammetric and spectroscopic data.
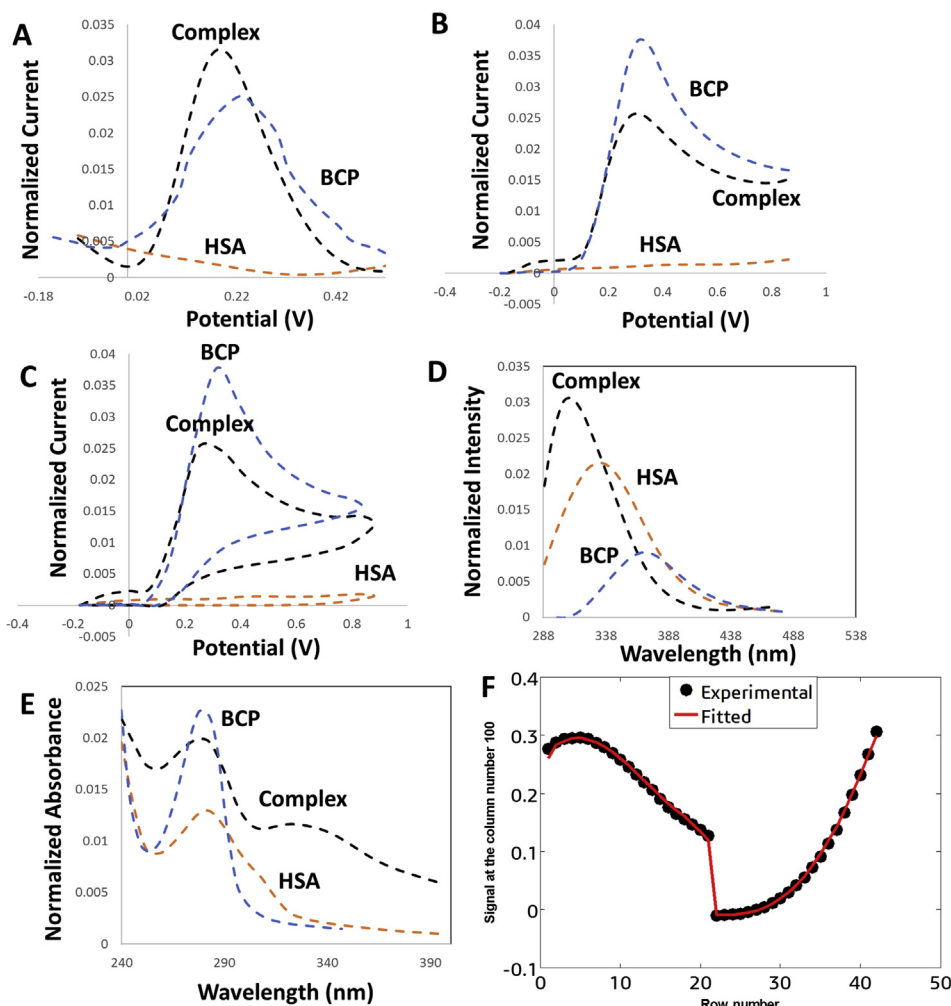
Fig. 7. (A)–(E) extracted signals of different species involved in DPV, LSV, CV, F and UVVis experiments, respectively, and (F) plot of coinciding experimental (points) and calculated data (line).

respectively. These observations confirm that the most intensity of complex formation is occurred at this ratio and which confirms that the complex specie is HSA-BCP$_2$. Therefore, according to the results of MCR-ALS, we can say that there are three species in the system studied here including free BCP, free HSA and a HSA-BCP$_2$ complex species. Pure voltammetric and spectral profiles resolved by MCR-ALS can be observed in Fig. 7A–E. Voltammetric profiles show that the HSA is electro-inactive while the complex specie is electroactive and this may be related to accessibility of the tryptophan and tyrosine residues of HSA by unfolding its structure upon reacting with BCP. Therefore, it can be concluded that embedding of two BCP molecules in HSA structure unfolds the HSA structure which opens the pathways for accessibility of tryptophan and tyrosine residues to be oxidizable at the electrode surface. A plot with coincided experimental and theoretical data which is shown in Fig. 7F by which the quality of the fitting process is guaranteed.

4.3.2. Application of MCR-BANDS to the verification of the MCR-ALS results

As stated in previous sections, application of constraints can help us to obtain meaningful results which is an important advantage of MCR rather than the other bilinear methods [59]. However, sometimes, MCR used a band of feasible solutions instead of a unique solution which may cause some ambiguities in the results [60]. Therefore, the presence of ambiguities in MCR-ALS results must be verified and MCR-BANDS as an efficient chemometric tool has been developed to calculate maximum and minimum of the relative contribution of the components to estimate

the feasible solutions [59, 61] which can help us to estimate the extent of rotational ambiguities [62]. In this work, to estimate the extent of rotational ambiguities in MCR-ALS results, the data matrix reproduced by MCR-ALS was used as the input of MCR-BANDS and analysed under the same constraints used for MCR-ALS. The maximum relative contribution function (f^{max}) and minimum relative contribution function (f^{min}) for each species were calculated: HSA ($f^{max} = 0.348$ and $f^{min} = 0.348$), BCP ($f^{max} = 0.291$ and $f^{min} = 0.291$) and HSA-BCP$_2$ ($f^{max} = 0.355$ and $f^{min} = 0.355$). As can be seen, there is no difference between the f^{max} and f^{min} for all the contributing species which confirm that there isn't any rotational ambiguity [59]. The good quality for the results of MCR-ALS are related to matrix augmentation and using suitable constraints for the resolution.

4.4. Hard-modeling

Four building a hard-model, definition of the stoichiometry of the

Table 3
Results of calculating binding constant by EQUISPEC.

Analyzed matrix	K_b
	HSA-BCP$_2$
$[\boldsymbol{D}_{DPV}^{BCP} \boldsymbol{D}_{LSV}^{BCP} \boldsymbol{D}_{CV}^{BCP} \boldsymbol{D}_{F}^{BCP} \boldsymbol{D}_{UVVis}^{BCP}]$	5.11×10^5
$[\boldsymbol{D}_{DPV}^{HSA} \boldsymbol{D}_{LSV}^{HSA} \boldsymbol{D}_{CV}^{HSA} \boldsymbol{D}_{F}^{HSA} \boldsymbol{D}_{UVVis}^{HSA}]$	5.29×10^5
$\begin{bmatrix} \boldsymbol{D}_{DPV}^{BCP} \boldsymbol{D}_{LSV}^{BCP} \boldsymbol{D}_{CV}^{BCP} \boldsymbol{D}_{F}^{BCP} \boldsymbol{D}_{UVVis}^{BCP} \\ \boldsymbol{D}_{DPV}^{HSA} \boldsymbol{D}_{LSV}^{HSA} \boldsymbol{D}_{CV}^{HSA} \boldsymbol{D}_{F}^{HSA} \boldsymbol{D}_{UVVis}^{HSA} \end{bmatrix}$	5.12×10^5

species and estimation of the binding constant are necessary and then, decomposition of data matrix D can be performed according to Eq. (1). The first step is focused on obtaining an estimation for the concentration profiles (C) and then, the pure spectra (S^T) can be calculated by least squares fitting with the best matching of C and D. The differences between input data matrix and the reproduced data matrix are gathered in the residual data matrix (E). Optimization procedure can be performed by the hard-modeling algorithm using tuning the defined stoichiometries to obtain a desired level of residuals. More details can be found in Ref. [63].

Here, EQUISPEC was used calculate the binding constants and the results are collected in Table 3. As can be seen, there is a good agreement between the results of EQUISPEC and those of Section 4.1.1.

4.5. Molecular docking

In this study, the Arguslab program was used to realize the binding mode of BCP at the active site of HSA. The main aspect for the ligand docking postures was considering the effective interaction of the drug with the various amino acid residues in the active site. The applied box size was $60 \times 60 \times 60$ Å and grid resolution was 0.4 Å. Docking simulations were performed by selecting ArgusDock as the docking engine flexible for the drug. Finally, the AScore was used as the scoring function and the results with different views are shown in Fig. 8A–C. The results showed that the binding sites were Lys 199, Tyr 214, Leu 198, Arg 218, Val 455, Lys 195, Arg 222, Asp 451, Ser 192, Pro 447, Tyr 452, Glu 292, His 288, Ala 191, Cys 448, Phe 157, Glu 188 and Lys 436. The ΔG was -29.01 kJ mol^{-1} and BCP was bound to sub-domain IIA of HSA. The LIGPLOT program was also used to more investigation of BCP-HSA interactions and the results are shown in Fig. 8D. LIPLOT shows the hydrophobic interactions and hydrogen bindings and according to its outputs three hydrogen bonds between BCP and Lys 436, BCP and Lys 195 and BCP and Arg 218 were observed and hydrophobic interactions were observed between BCP and Glu 188, Ser 192, Glu 292, Ala 191, Trp 214, Val 455, Tyr 452 and Cys 448.

4.6. Analytical characterizations

The aim of this section is to develop a novel electroanalytical methodology for sensitive determination of HSA based on BCP-HSA interactions. To achieve more sensitivity amperometric measurements were chosen and the GCE was modified [64, 65, 66, 67, 68, 69].

4.6.1. Amperometric measurements

For electrochemical biosensing of the electro-inactive HSA, two different amperometric experiments were performed in the absence and presence of HSA. One amperometric measurement was performed under addition of nineteen different concentrations of BCP ranging in 2–100 μM upon applying a potential of 0.12 V (oxidation potential of BCP at the surface of MWCNTs-IL/GCE) and the related *i-t* data were depicted in Fig. 9A. The second amperometric experiment was performed by the addition of BCP with the same concentrations used for the first experiment but in the presence of increasing concentration of HSA in the range of 2–98 nM. The *i*-t* curve related to the second experiment is depicted in Fig. 9B. A calibration curve for electrochemical biosensing of HSA was built based on regression of $\Delta i = i\text{-}i^*$ values HSA concentration which can be seen in Fig. 9C. Two linear ranges including 2–16 nM and 16–98 nM were obtained and sensitivity and limit of detection (LOD) of the sensor were calculated to be 2.15 μA nM^{-1} and 1 nM (according to $3SD/m$, where SD is the standard deviation of the intercept and m is the slope of the calibration curve), respectively.

4.6.2. Interference study

In order to investigate the selectivity of the sensor response to HSA in the presence of interfering species, its response to 10 nM HSA in the presence of 100-fold interfering species including (a) cysteine, (b) tyrosine, (c) histidine, (d) valine, (e) methionine, (f) proline, (g) phenylalanine, (h) egg albumin, (i) chloramphenicol, (j) amoxicillin, (k) vitamin C and (l) vitamin B12 was examined and the results are shown in Fig. 9D. The results showed that the sensor had a selective response to HSA.
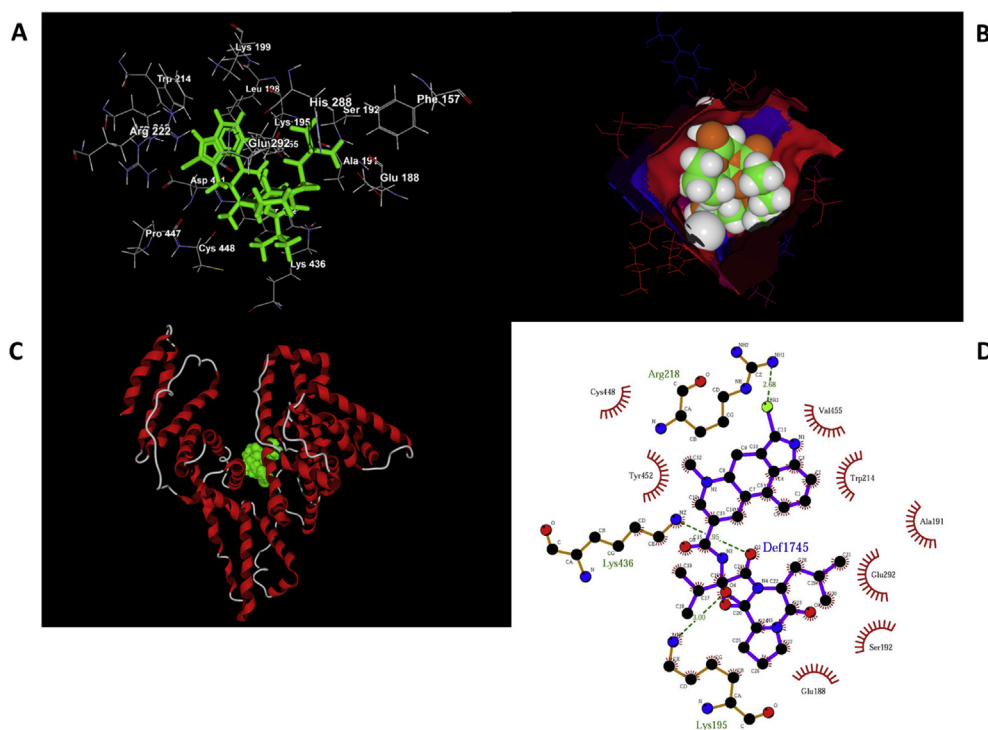

Fig. 8. Computer-generated models of binding BCP to HSA presented by: (A) pose organizer view, (B) hydrophobicity view and (C) secondary structure view. (D) BCP-HSA interactions presented by LigPlot program.
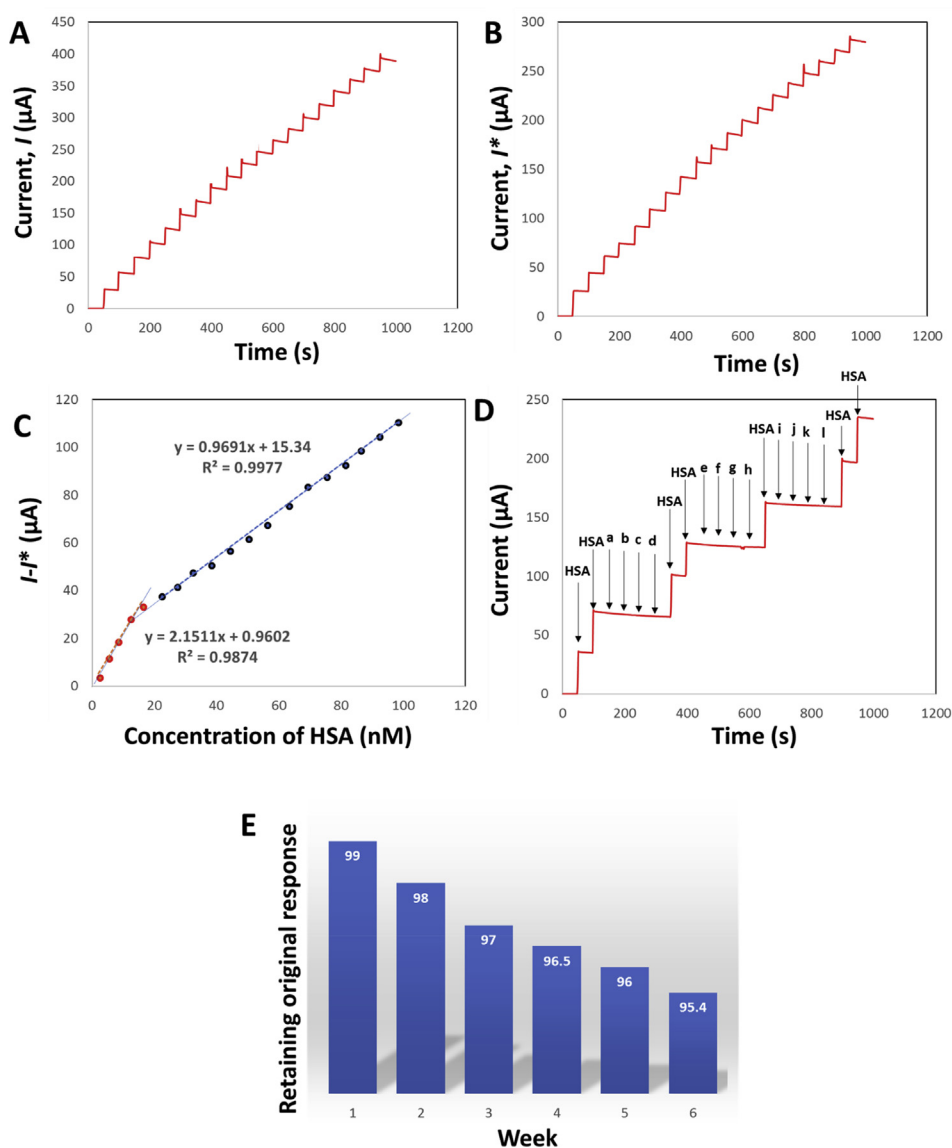
Fig. 9. (A) Amperometric responses recorded by MWCNTs-IL/GCE upon increasing concentration of BCP, (B) same as (A) but, in the presence of increasing concentration of HSA, (C) regression of $\Delta i = i\text{-}i^*$ values on concentrations of HSA, first range: $\Delta i = 2.1511 C_{HSA} + 0.9602$, $R^2 = 0.9874$, second range: $\Delta i = 0.9691 C_{HSA} + 15.34$, $R^2 = 0.9977$, (D) amperometric responses of the sensor to HSA and interfering species and (E) examination of the stability of the sensor response to HSA by weekly measurement of its response during six weeks.

4.6.3. Stability, repeatability and reproducibility

Stability of a newly developed sensor is a critical characteristic which must be investigated before advising its capability for the analysis of real samples. Therefore, to achieve this goal, the sensor was applied to the determination of 70 nM HSA for six weeks and its response was weekly recorded and the data are shown in Fig. 9E. The results showed that the sensor retained 95.4% of its original response which guaranteed the stability of the sensor. The response of the sensor to 70 nM HSA was also examined for ten times during a day and our records confirmed a good relative standard deviation (RSD) value of 3.33% which confirmed a repeatable response for the sensor. The next attempt was focused on the examination of the reproducibility of the sensor and to achieve this goal, six sensors fabricated by the same procedure were applied to the determination of 70 nM HSA. The RSD value was calculated to be 3.78% which suggested a reproducible response for the developed sensor in this study.

4.6.4. Validation of the developed method

In this section, the sensor was applied to the analysis of real samples and its results were compared with a reference method based on capillary electrophoresis. The results are presented in Table 4. As can be seen, the results obtained by the two methods are in a good agreement.

Table 4
Results of the analysis of human serum samples by the reference method and proposed method in this study.

Sample	Found by the proposed method in this study ($n = 4$)	Found by the reference method ($n = 4$)
Serum 1	$6.91\ (\pm0.05) \times 10^{-4}$ M	$7.01\ (\pm0.03) \times 10^{-4}$ M
Serum 2	$7.11\ (\pm0.04) \times 10^{-4}$ M	$7.08\ (\pm0.02) \times 10^{-4}$ M
Serum 3	$7.54\ (\pm0.02) \times 10^{-4}$ M	$7.77\ (\pm0.05) \times 10^{-4}$ M

5. Conclusions

In the present study, BCP-HSA interactions were investigated by experimental and theoretical methods. The first attempt was focused on recording electrochemical and spectroscopic data to obtain some information about the mentioned interactions. Then, electrochemical and spectroscopic data were combined to build an augmented data matrix which were analysed by MCR-ALS to obtain more information which could not be obtained by direct analysis of the data. The next attempt was focused on modeling of the interactions of BCP with HSA by molecular

docking methods and the outputs of this section was used to verify the results of experimental sections. Finally, a novel method based on BCP-HSA interactions was developed for sensitive electrochemical determination of electro-inactive HSA. This study was a thorough which traveled from bio-interaction to biosensing and definitely will be extended in future to develop more interesting studies.

Declarations

Author contribution statement

Ali R. Jalalvand: Conceived and designed the experiments; Performed the experiments.

Sirous Ghobadi: Performed the experiments; Contributed reagents, materials, analysis tools or data.

Hector C. Goicoechea: Analyzed and interpreted the data; Contributed reagents, materials, analysis tools or data.

Elahe Faramarzi: Performed the experiments; Analyzed and interpreted the data.

Majid Mahmoudi: Contributed reagents, materials, analysis tools or data; Wrote the paper.

Funding statement

Competing interest statement

The authors declare no conflict of interest.

Additional information

No additional information is available for this paper.

References

[1] US Pharmacopoeia, US Convention, Rockville, MD, 2004.
[2] D. Parkes, in: N.J. Harper, A.B. Simmonds (Eds.), Advances in Drug Research, Academic Press, New York, 1977.
[3] H.P. Weber, in: M. Goldstein (Ed.), Ergot Compounds and Brain Function: Neuroendocrine and Neuropsychiatric Aspects, Raven Press, New York, 1980.
[4] K.Y. Ho, M.O. Thorner, Therapeutic applications of bromocriptine in endocrine and neurological diseases, Drugs 36 (1988) 67–82.
[5] F. Marzatico, C. Cafe, M. Taborelli, G. Benzi, Experimental Parkinson's disease in monkeys. Effect of ergot alkaloid derivative on lipid peroxidation in different brain areas, Neurochem. Res. 18 (1993) 1101–1106.
[6] E. Del Pozo, L. Varga, H. Wyss, G. Tolis, H. Friesen, R. Wenner, L. Vetter, A. Uettwiler, Clinical and hormonal response to bromocriptin (CB-154) in the galactorrhea syndromes, J. Clin. Endocrinol. Metab. 39 (1974) 18–26.
[7] C.Q. Earl, W.C. Prozialeck, B. Weiss, Interaction of alpha adrenergic antagonists with calmodulin, Life Sci. 35 (1984) 525–534.
[8] B. Weiss, W.C. Prozialeck, T.L. Wallace, Interaction of drugs with calmodulin. Biochemical, pharmacological and clinical implications, Biochem. Pharmacol. 31 (1982) 2217–2226.
[9] M.B. Gholivand, A.R. Jalalvand, H.C. Goicoechea, M. Omidi, Investigation of interaction of nuclear fast red with human serum albumin by experimental and computational approaches, Spectrochim. Acta A 115 (2013) 354–365.
[10] M.B. Gholivand, A.R. Jalalvand, H.C. Goicoechea, R. Gargallo, T. Skov, Chemometrics: an important tool for monitoring interactions of vitamin B7 with bovine serum albumin with the aim of developing an efficient biosensing system for the analysis of protein, Talanta 132 (2015) 354–365.
[11] M.B. Gholivand, A.R. Jalalvand, H.C. Goicoechea, T. Skov, Fabrication of an ultrasensitive impedimetric buprenorphine hydrochloride biosensor from computational and experimental angles, Talanta 124 (2014) 27–35.
[12] M.B. Gholivand, A.R. Jalalvand, H.C. Goicoechea, Developing a novel computationally designed impedimetric pregabalin biosensor, Electrochim. Acta 133 (2014) 123–131.
[13] M.B. Gholivand, A.R. Jalalvand, G. Paimard, H.C. Goicoechea, T. Skov, R. Farhadi, S. Ghobadi, N. Moradi, V. Nasirian, Fabrication of a novel naltrexone biosensor based on a computationally engineered nanobiocomposite, Int. J. Biol. Macromol. 70 (2014) 596–605.
[14] A.R. Jalalvand, S. Ghobadi, H.C. Goicoechea, H.W. Gu, E. Sanchooli, Investigation of interactions of Comtan with human serum albumin by mathematically modeled

[15] voltammetric data: a study from bio-interaction to biosensing, Bioelectrochemistry 123 (2018) 162–172.
[15] G. Mohammadi, E. Faramarzi, M. Mahmoudi, S. Ghobadi, A.R. Ghiasvand, H.C. Goicoechea, A.R. Jalalvand, Chemometrics-assisted investigation of interactions of Tasmar withhuman serum albumin at a glassy carbon disk: application toelectrochemical biosensing of electro-inactive serum albumin, J. Pharm. Biomed. Anal. 156 (2018) 23–35.
[16] Y.Y. Yue, X.G. Chen, J. Qin, X.J. Yao, Characterization of the mangiferin–human serum albumin complex by spectroscopic and molecular modeling approaches, J. Pharm. Biomed. Anal. 49 (2009) 753–759.
[17] J.S. Mandeville, E. Froehlich, H.A. Tajmir-Riahi, Study of curcumin and genistein interactions with human serum albumin, J. Pharm. Biomed. Anal. 49 (2009) 468–474.
[18] H.X. Luo, Y. Du, Z.X. Guo, Electrochemistry of N-n-undecyl-N′-(sodium-p-aminobenzenesulfonate) thiourea and its interaction with bovine serum albumin, Bioelectrochemistry 74 (2009) 232–235.
[19] Q.H. Lu, C.D. Ba, D.Y. Chen, Investigating noncovalent interactions of rutin – serum albumin by capillary electrophoresis – frontal analysis, J. Pharm. Biomed. Anal. 47 (2008) 888–891.
[20] C. Bertucci, V. Andrisano, R. Gotti, V. Cavrini, Use of an immobilised human serum albumin HPLC column as a probe of drug–protein interactions: the reversible binding of valproate, J. Chromatogr. B 768 (2002) 147–155.
[21] B. Bojko, A. Sulkowska, M. Maciazek-Jurczyk, J. Rownicka, W.W. Sulkowski, Investigations of acetaminophen binding to bovine serum albumin in the presence of fatty acid: fluorescence and 1H NMR studies, J. Mol. Struct. 924–926 (2009) 332–337.
[22] Y.N. Ni, S.S. Wang, S. Kokot, Spectrometric study of the interaction between Alpinetin and bovine serum albumin using chemometrics approaches, Anal. Chim. Acta 663 (2010) 139–146.
[23] Y.N. Ni, G.L. Liu, S. Kokot, Fluorescence spectrometric study on the interactions of Isoprocarb and sodium 2-isopropylphenate with bovine serum albumin, Talanta 76 (2008) 513–521.
[24] A.C. Wallace, R.A. Laskowski, J.M. Thornton, LIGPLOT: a program to generate schematic diagrams of protein-ligand interactions, Protein Eng. 8 (1995) 127–134.
[25] http://www.ub.es/gesq/mcr/mcr.htm.
[26] M.B. Gholivand, A.R. Jalalvand, H.C. Goicoechea, Multivariate analysis for resolving interactions of carbidopa with dsDNA at a fullerene-C_{60}/GCE, Int. J. Biol. Macromol. 69 (2014) 369–381.
[27] A.R. Jalalvand, H.C. Goicoechea, D.N. Rutledge, Applications and challenges of multi-way calibration in electrochemical analysis, Trends Anal. Chem. 87 (2017) 32–48.
[28] A.R. Jalalvand, H.C. Goicoechea, Applications of electrochemical data analysis by multivariate curve resolution-alternating least squares, Trends Anal. Chem. 88C (2017) 134–166.
[29] K. Ghanbari, M. Roushani, F. Farzadfar, H.C. Goicoechea, A.R. Jalalvand, Developing a four-dimensional voltammetry as a powerful electroanalytical methodology for simultaneous determination of three colorants in the presence of an uncalibrated interference, Chemometr. Intell. Lab. Syst. 189 (2019) 27–38.
[30] H. Gampp, M. Maeder, C.J. Meyer, A.D. Zuberbühler, Calculation of equilibrium constants from multiwavelength spectroscopic data—III: model-free analysis of spectrophotometric and ESR titrations, Talanta 32 (1985) 1133–1139.
[31] H. Abdollahi, V. Mahdavi, Tautomerization equilibria in aqueous micellar Solutions: a spectrophotometric and factor-analytical study, Langmuir 23 (2007) 2362–2368.
[32] S. Perez, M.J. Culzoni, G.G. Siano, M.D. Gil Garcia, H.C. Goicoechea, M.M. Galera, Detection of unintended stress effects based on a metabonomic study in tomato fruits after treatment with carbofuran pesticide. capabilities of MCR-ALS applied to LC-MS three-way data arrays, Anal. Chem. 81 (2009) 8335–8346.
[33] M. Vives, R. Gargallo, R. Tauler, Study of the intercalation equilibrium between the polynucleotide poly(adenylic)-poly(uridylic) acid and the ethidium bromide dye by means of multivariate curve resolution and the multivariate extension of the continuous variation and mole ratio methods, Anal. Chem. 71 (1999) 4328–4337.
[34] C.B. Zachariassen, J. Larsen, F. Van den Berg, R. Bro, A. De Juan, R. Tauler, Comparison of PARAFAC2 and MCR-ALS for resolution of an analytical liquid dilution system, Chemometr. Intell. Lab. Syst. 83 (2006) 13–25.
[35] R. Tauler, A. Izquierdo-Ridorsa, E. Casassas, Simultaneous analysis of several spectroscopic titrations with self-modelling curve resolution, Chemometr. Intell. Lab. Syst. 18 (1993) 293–300.
[36] R. Tauler, A.K. Smilde, B.R. Kowalski, Selectivity, local rank, three-way data analysis and ambiguity in multivariate curve resolution, J. Chemom. 9 (1995) 31–58.
[37] M. Esteban, C. Arino, J.M. Dıaz-Cruz, M.S. Diaz-Cruz, R. Tauler, Multivariate curve resolution with alternating least squares optimisation: a soft-modelling approach to metal complexation studies by voltammetric techniques, Trends Anal. Chem. 19 (2000) 49–61.
[38] M. Esteban, C. Arino, J.M. Dıaz-Cruz, Chemometrics for the analysis of voltammetric data, Trends Anal. Chem. 25 (2006) 86–92.
[39] R.N. Goyal, A.B. Toth, G. Dryhurst, N.T. Nguyen, A comparison of the peroxidase-catalyzed and electrochemical oxidation of uric acid, Bioelectrochem. Bioenerg. 9 (1982) 39–60.
[40] Y.N. Ni, X. Zhang, S. Kokot, Spectrometric and voltammetric studies of the interaction between quercetin and bovine serum albumin using warfarin as site marker with the aid of chemometrics, Spectrochim. Acta A 71 (2009) 1865–1872.
[41] A.J. Bard, L.R. Faulkner, Electrochemical Methods: Fundamentals and Applications, second ed., Wiley, New York, 2001.

[42] E. Laviron, Adsorption, autoinhibition and autocatalysis in polarography and in linear potential sweep voltammetry, J. Electroanal. Chem. 52 (1974) 355–393.

[43] H. Heli, N. Sattarahmady, A. Jabbari, A.A. Moosavi-Movahedi, G.H. Hakimelahi, F.Y. Tsai, Adsorption of human serum albumin onto glassy carbon surface-Applied to albumin-modified electrode: mode of protein-ligand interactions, J. Electroanal. Chem. 610 (2007) 67–74.

[44] V. Brabec, DNA sensor for the determination of antitumor platinum compounds, Electrochim. Acta 45 (2000) 2929–2932.

[45] X. Ju, Y.K. Ye, Y.L. Zhu, Interaction between nile blue and immobilized single- or double-stranded DNA and its application in electrochemical recognition, Electrochim. Acta 50 (2005) 1361–1367.

[46] S.S. Kalanur, U. Katrahalli, J. Seetharamappa, Electrochemical studies and spectroscopic investigations on the interaction of an anticancer drug with DNA and their analytical applications, J. Electroanal. Chem. 636 (2009) 93–100.

[47] B. Ojiha, G. Das, The interaction of 5-(Alkoxy)naphthalen-1-amine with bovine serum albumin and its effect on the conformation of protein, J. Phys. Chem. B 114 (2010) 3979–3986.

[48] D.M. Charbonneau, H.A. Tajmir-RIAHI, Study on the interaction of cationic lipids with bovine serum albumin, J. Phys. Chem. B 114 (2010) 1148–1155.

[49] Y. Yue, Z. Wang, Z. Wang, Y. Zhang, J. Liu, A comparative study of binding properties of different coumarin-based compounds with human serum albumin, J. Mol. Struct. 1169 (2018) 75–80.

[50] J. Liu, X. Yang, Y. Yue, S. Zhao, Investigation of the interaction of aurantio-obtusin with human serum albumin by spectroscopic and molecular docking methods, Luminescence 33 (2018) 104–111.

[51] J.R. Lakowicz, Principles of Fluorescence Spectroscopy, second ed., Plenum Press, New York, 1999.

[52] M.A. Khan, S. Muzammil, J. Musarrat, Interaction of genome-linked protein (VPg) of turnip mosaic virus with wheat germ translation initiation factors eIFiso4E and eIFiso4F, Int. J. Biol. Macramol. 30 (2002) 243–249.

[53] G. Sudlow, D.J. Birkett, D.N. Wade, Further characterization of specific drug binding sites on human serum albumin, Mol. Pharmacol. 12 (1976) 1052–1061.

[54] L. Stryer, R.P. Haugland, Energy transfer: a spectroscopic ruler, Proc. Natl. Acad. Sci. U.S.A. 58 (1967) 719–726.

[55] B. Valeur, J.C. Brochon, New Trends in Fluorescence Spectroscopy, third ed., Springer, Berlin, 2001.

[56] F.L. Cui, J. Fan, J.P. Li, Z.D. Hu, Interactions between 1-benzoyl-4-p-chlorophenyl thiosemicarbazide and serum albumin: investigation by fluorescence spectroscopy, Bioorg. Med. Chem. 12 (2004) 151–157.

[57] B. Valeur, Molecular Fluorescence: Principles and Applications, Wiley, New York, 2001.

[58] A. de Juan, A. Izquierdo-Ridorsa, R. Tauler, G. Fonrodona, E. Casassas, A soft-modeling approach to interpret thermodynamic and conformational transitions of polynucleotides, Biophys. J. 73 (1997) 2937–2948.

[59] J. Jaumot, R. Tauler, MCR-BANDS: a user friendly MATLAB program for the evaluation of rotation ambiguities in Multivariate Curve Resolution, Chemometr. Intell. Lab. Syst. 103 (2010) 96–107.

[60] H. Abdollahi, R. Tauler, Uniqueness and rotation ambiguities in multivariate curve resolution methods, Chemometr. Intell. Lab. Syst. 108 (2011) 100–111.

[61] R. Tauler, Calculation of maximum and minimum band boundaries of feasible solutions for species profiles obtained by multivariate curve resolution, J. Chemom. 15 (2001) 627–646.

[62] H. Parastar, M. Jalali-Heravi, R. Tauler, Is independent component analysis appropriate for multivariate resolution in analytical chemistry? Trends Anal. Chem. 31 (2012) 134–143.

[63] R.M. Dyson, S. Kaderli, G.A. Lawrance, M. Maeder, A.D. Zuberbühler, Second order global analysis: the evaluation of series of spectrophotometric titrations for improved determination of equilibrium constants, Anal. Chim. Acta 353 (1997) 381–393.

[64] A.R. Jalalvand, A. Haseli, F. Farzadfar, H.C. Goicoechea, Fabrication of a novel biosensor for biosensing of bisphenol A and detection of its damage to DNA, Talanta 201 (2019) 350–357.

[65] A.R. Jalalvand, Fabrication of a novel and ultrasensitive label-free electrochemical aptasensor for detection of biomarker prostate specific antigen, Int. J. Biol. Macromol. 126 (2019) 1065–1073.

[66] A.R. Jalalvand, M.-B. Gholivand, H.C. Goicoechea, T. Skov, K. Mansouri, Mimicking enzymatic effects of cytochrome P450 by an efficient biosensor for in vitro detection of DNA damage, Int. J. Biol. Macromol. 79 (2015) 1004–1010.

[67] M.-B. Gholivand, A.R. Jalalvand, H.C. Goicoechea, G. Paimard, T. Skov, Surface exploration of a room-temperature ionic liquid-chitin composite film decorated with electrochemically deposited PdFeNi trimetallic alloy nanoparticles by pattern recognition: an elegant approach to developing a novel biotin biosensor, Talanta 131 (2015) 249–258.

[68] M.-B. Gholivand, A.R. Jalalvand, H.C. Goicoechea, Computer-assisted electrochemical fabrication of a highly selective and sensitive amperometric nitrite sensor based on surface decoration of electrochemically reduced graphene oxide nanosheets with CoNi bimetallic alloy nanoparticles, Mater. Sci. Eng. C 40 (2014) 109–120.

[69] R. Khodarahmi, S. Khateri, H. Adibi, V. Nasirian, M. Hedayati, E. Faramarzi, S. Soleimani, H.C. Goicoechea, A.R. Jalalvand, Chemometrical-electrochemical investigation for comparing inhibitory effects of quercetin and its sulfonamide derivative on human carbonic anhydrase II: theoretical and experimental evidence, Int. J. Biol. Macromol. 136 (2019) 377–385.